Faraday Discussions

Cite this: *Faraday Discuss.*, 2014, **168**, 449

PAPER

View Article Online
View Journal | View Issue

Cold condensation of dust in the ISM

Gaël Rouillé,[a] Cornelia Jäger,*[a] Serge A. Krasnokutski,[a] Melinda Krebsz[b] and Thomas Henning[c]

Received 12th February 2014, Accepted 13th February 2014
DOI: 10.1039/c4fd00010b

The condensation of complex silicates with pyroxene and olivine composition under conditions prevailing in molecular clouds has been experimentally studied. For this purpose, molecular species comprising refractory elements were forced to accrete on cold substrates representing the cold surfaces of surviving dust grains in the interstellar medium. The efficient formation of amorphous and homogeneous magnesium iron silicates at temperatures of about 12 K has been monitored by IR spectroscopy. The gaseous precursors of such condensation processes in the interstellar medium are formed by erosion of dust grains in supernova shock waves. In the laboratory, we have evaporated glassy silicate dust analogs and embedded the released species in neon ice matrices that have been studied spectroscopically to identify the molecular precursors of the condensing solid silicates. A sound coincidence between the 10 μm band of the interstellar silicates and the 10 μm band of the low-temperature siliceous condensates can be noted.

1 Introduction

AGB stars and supernovae (SNs) are main cosmic dust factories. The formed stardust is finally distributed into the interstellar medium (ISM), and eventually becomes a part of cold and dense molecular clouds. Interstellar dust is exposed to destructive processes caused by supernova-induced shock waves. It was estimated that only a few percent of the total mass of stardust survive these destructive processes in the ISM.[1,2] However, observations of refractory elements in the ISM clearly show a depletion of these elements from the gas phase. Consequently, an efficient condensation process of dust grains in the ISM is required to balance the discrepancy between the stellar formation of dust grains and their interstellar destruction.[2] Recently, Jones & Nuth[3] discussed a compatible injection and

[a]*Laboratory Astrophysics Group of the Max Planck Institute for Astronomy at the Friedrich Schiller University Jena, Institute of Solid State Physics, Helmholtzweg 3, 07743 Jena, Germany. E-mail: cornelia.jaeger@uni-jena.de; Fax: +49-3641-9-47308; Tel: +49-3641-9-47354*

[b]*Institute for Geological and Geochemical Research, Research Centre for Astronomy and Earth Sciences, Hungarian Academy of Sciences, 45 Budaörsi street, 1112 Budapest, Hungary*

[c]*Max Planck Institute for Astronomy, Königstuhl 17, 69117 Heidelberg, Germany*

destruction time scale for silicate dust particles, an assumption based on inherent uncertainties in the determination of destruction efficiencies.

In the ISM, refractory and other atoms and molecules generated by the erosion of grains in supernova shocks slowly accrete onto surfaces of surviving grains at low temperatures. This process is suggested to occur in the very dense cores of molecular clouds (MCs) where the temperature of dust grains is between 10 and 20 K. However, such processes may already occur in the outer, less dense regions of molecular clouds. The accreted species can finally react among each other to form solid layers on the grains. In the very dense cores of MCs, other abundant gaseous species such as CO, H_2O, and small carbon-rich molecules simultaneously accrete with refractory species and may prevent the formation of refractory silicate material. However, fast desorption processes of carbon-based condensates may also lead to a preferred formation of silicate condensates and to a separation of siliceous and carbonaceous dust in the ISM.

Very recently, the condensation of SiO molecules at low temperature using neon matrix and helium droplet isolation techniques has been studied.[4] SiO represents the major component of the interstellar silicates. Reactions between SiO molecules were found to be barrierless. The energy of SiO polymerization reactions has been determined experimentally using a calorimetric method, and theoretically with calculations based on the coupled-cluster and density functional theories. The experiments have clearly revealed the efficient formation of SiO_x condensates at temperatures of about 10 K.[4]

In the present work, we extend our recently performed experimental studies on the cold condensation process of SiO to more complex systems containing magnesium and iron. This step is necessary to obtain more insight into the low-temperature condensation process of realistic interstellar silicates. We apply laser vaporization to silicate samples in an attempt to produce the precursor species involved in the condensation of interstellar silicates. In a first stage, the vaporized species are deposited and isolated in a Ne matrix where they are cooled down to temperatures relevant to the ISM. This stage gives us the opportunity to identify the laser-vaporized species by absorption spectroscopy in the UV and mid-IR wavelength domains. The second stage consists of annealing and warming the matrix up to 13 K until the complete evaporation of the Ne atoms, in order to cause the accretion of the laser-vaporized species at low temperature.

2 Experimental

Chunks of two amorphous silicates, synthesized in-house by melting and quenching,[5] were used as targets. The formula of one silicate was Mg_2SiO_4, corresponding to the stoichiometry of forsterite, the Mg endmember of the olivine group. The formula of the other silicate was $Mg_{0.4}Fe_{0.6}SiO_3$, *i.e.*, the composition of a pyroxene.

Laser vaporization was carried out using a pulsed laser source (Continuum Minilite II) emitting photons with a wavelength of 532 nm. The laser was operated with a repetition rate of 10 pulses per second. Each pulse lasted 5 ns and carried an energy of 20 to 25 mJ. The laser beam was focused at the surface of the target and, during the experiments, it was shifted every minute to vaporize a fresh part of the target and also to avoid drilling through it. Holes 0.4 to 0.5 mm in diameter were created during the experiments. Assuming this diameter coincides with the

diameter of the laser beam at the target position, a fluence of 2 to 4 GW cm^{-2} is inferred.

Matrix isolation spectroscopy was performed with Ne (Linde, purity 99.995%) as the matrix material. Each matrix was grown on a KBr substrate (Korth Kristalle GmbH). This material transmits photons in the mid-IR wavelength domain and also at useful UV wavelengths, with a lower limit of 205 nm. A compressed-He closed-cycle cryocooler (Advanced Research Systems Inc. DE-204SL) was employed to cool down the substrate and to maintain it at low temperature. In order to form a Ne matrix, the substrate was kept at ~6 K and the Ne mass flow rate was set to 5 standard cubic centimeters per minute. The target for laser vaporization and the substrate were separated by a distance of ~55 mm.

The cryocooler could be rotated while being operated, allowing the substrate to face three directions and the corresponding pairs of opposite ports that equipped the vacuum chamber. These ports allowed us, in turn, to deposit the Ne atoms and laser-vaporized species on the substrate, to measure IR spectra and UV spectra in transmission. A Fourier transform IR spectrometer (Bruker VERTEX 80v) and a UV spectrometer (JASCO V-670 EX) were optically coupled to the vacuum chamber. The IR beam of the FTIR spectrometer, guided along an evacuated optical path by means of gold-coated mirrors, passed through the vacuum chamber to reach an external detector. Optical fibers fitted with collimating optics were used to carry the photons from the UV spectrometer to the vacuum chamber and back.

The IR spectra were measured by averaging 64 scans carried out at a speed of 10 kHz with a resolution of 1 cm^{-1}. The UV spectra were measured with equal step and resolution of 0.2 nm at a rate of ~11 nm min^{-1}.

3 Results

3.1 Analysis of the evaporated species

The isolation of the vaporized species in the Ne matrices gives us the opportunity to identify them using absorption spectroscopy, and also to verify the presence of contaminants. For instance, our spectra show bands due to the Ne matrix-isolated contaminants CO (2141 cm^{-1}),[6] CO_2 (2348 cm^{-1}),[7] H_2O (line systems at 1631 and 3783 cm^{-1}),[8] and $(H_2O)_2$ (lines at 3590 and 3734 cm^{-1}).[8]

3.1.1 Mg_2SiO_4 target. Magnesium atoms are easily detected in the UV region. In Fig. 1, the line of atomic Mg at 275 nm is very strong, indicating the efficient vaporization of this element. Allowing for a matrix-induced wavelength shift, this line corresponds to that measured at 285.30 nm in vacuum.[9] Despite the large amount of Mg atoms, dimers are not observed. They would give rise to a band at ~257 nm corresponding to the $B^1\Pi_u \leftarrow X^1\Sigma_g^+$ transition.[10,11] A spectrum of Mg atoms deposited in a Ne matrix to serve as a reference supports the assignment.

Still at UV wavelengths, the peaks in a very weak, structured feature originating at 234 nm correspond to bands of the $A^1\Pi \leftarrow X^1\Sigma^+$ transition of the SiO molecule.[4,12] Thus only a very little amount of this species was deposited in the Ne matrix. Accordingly, features recently attributed to SiO oligomers, which are produced by barrierless reactions between the SiO molecules, are not found.[4]

In the 205 to 350 nm range, Si atoms in their ground state give medium to strong absorption lines at 220.87, 243.95, and 251.51 nm in vacuum.[9] These lines

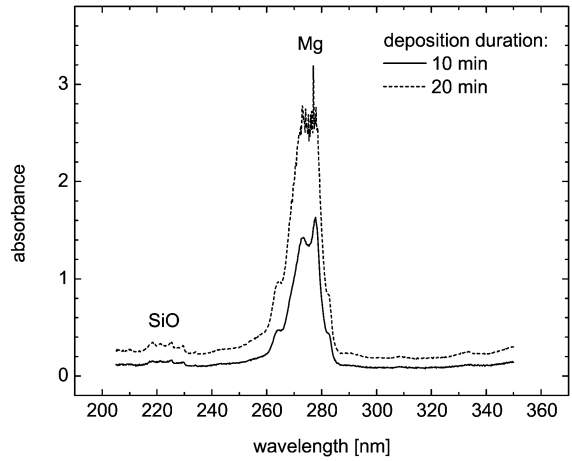

Fig. 1 Ultraviolet absorption features of species isolated in a Ne matrix at 6.3 K following laser vaporization of amorphous Mg_2SiO_4. The features are attributed to SiO and Mg. The absorption line of Mg is saturated after accumulating material for 20 min.

are not seen in our spectrum, even considering matrix-induced wavelength shifts. In the same region, O I atoms have only one very weak transition.

In the mid-IR domain, shown in Fig. 2, weak absorption bands arise at 913, 1039, 1107, 1164, 1228, 1754, 2152, and 2192 cm^{-1}. We assign the absorption bands seen at 1039 and 1107 cm^{-1} to the ν_3 and ν_1 modes of O_3, respectively.[13] Another band due to O_3 is not seen at 2109 cm^{-1} ($\nu_1 + \nu_3$),[13] most likely because being a combination band it is too weak. The identification of O_3 could have been confirmed by the observation of the broad Hartley band in the UV spectrum, near 253 nm.[14] This band, however, is not observed. The comparison between the

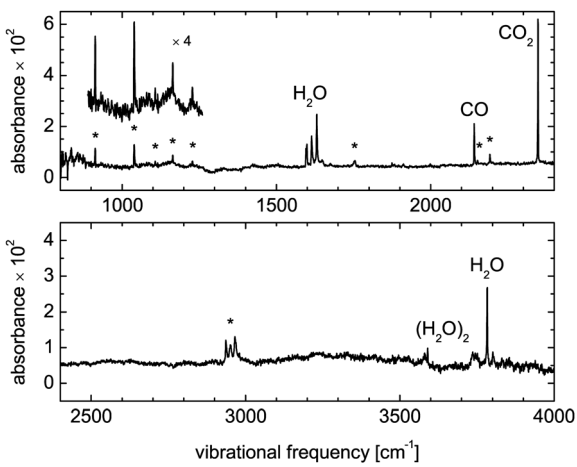

Fig. 2 Infrared absorption features of species isolated in a Ne matrix at 6.3 K following laser vaporization of amorphous Mg_2SiO_4. Asterisks mark the features of interest. The material had been accumulated for 20 min.

absorption cross-sections of the UV and IR transitions would clarify our assignment. The peak at 1164 cm^{-1} is attributed to O_4^+.[15,16] Those at 913 and 2192 cm^{-1} were recently reported and discussed by Jacox and Thompson.[17] It was found that these absorptions may be caused by a single species, which would be a molecular complex involving H_2 and possibly H_3O^+ or $H_2O_5^+$.

The line found at 1228 cm^{-1} is attributed to SiO.[18,19] As expected from the analysis of the UV spectrum, the IR bands that characterize the oligomers Si_2O_2 and Si_3O_3 are not seen.[18–20] Absorptions that would possibly reveal the presence of magnesium oxides lie at wavelengths longer than 10 μm, outside the range we have scanned.[21]

Finally, a tight group of bands that arises at 2937, 2951, and 2966 cm^{-1} resembles the bands of the ν_2 mode of H_2O near 1620 cm^{-1},[8] with a positive shift of 1337 cm^{-1}. The bands at 1754 and 2152 cm^{-1} remain unassigned.

3.1.2 $Mg_{0.4}Fe_{0.6}SiO_3$ target. In the UV region, shown in Fig. 3, the lines of the Fe and Mg atoms are strong, demonstrating again the efficient vaporization of magnesium, as observed with the Mg_2SiO_4 target, and also that of iron. Only a weak contribution of SiO is possibly detected. The lines assigned to Fe I are favorably compared with the vacuum wavelengths.[9] A spectrum of Fe atoms deposited in a Ne matrix was measured to serve as a reference, which supports the assignment. One can note that there is no evidence of the broad Hartley band of O_3.

In the IR spectrum displayed in Fig. 4, we find bands already observed when using the Mg_2SiO_4 target. Thus O_3 (1039 cm^{-1}), O_4^+ (1164 cm^{-1}), and SiO (1228 cm^{-1}) are present in the matrix. The band assigned above to the ν_1 mode of O_3 is absent. On the other hand, new bands of O_4^+ isomers are detected at 1321 and 2808 cm^{-1}.[15,16] The absorptions caused by a complex possibly involving H_2 and possibly H_3O^+ or $H_2O_5^+$ are also detected.[17]

There is no evidence again of the Si_2O_2 and Si_3O_3 oligomers. The unassigned peaks found at 1754 and 2152 cm^{-1} in the experiment with the Mg_2SiO_4 target are absent, like the group of bands previously observed around 2950 cm^{-1}.

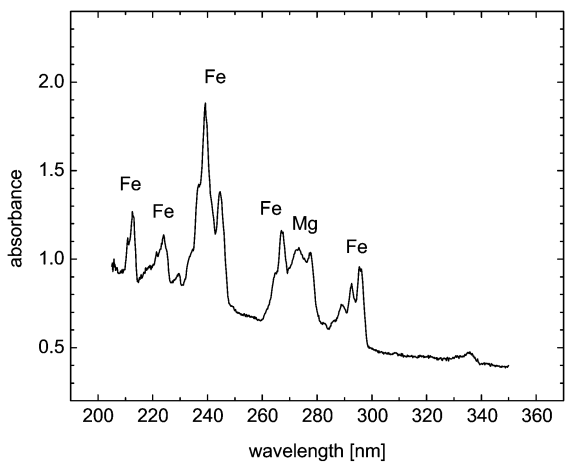

Fig. 3 Ultraviolet absorption features of species isolated in a Ne matrix at 6.3 K following laser vaporization of amorphous $Mg_{0.4}Fe_{0.6}SiO_3$. The features are attributed to Fe and Mg atoms. The material had been accumulated for 20 min.

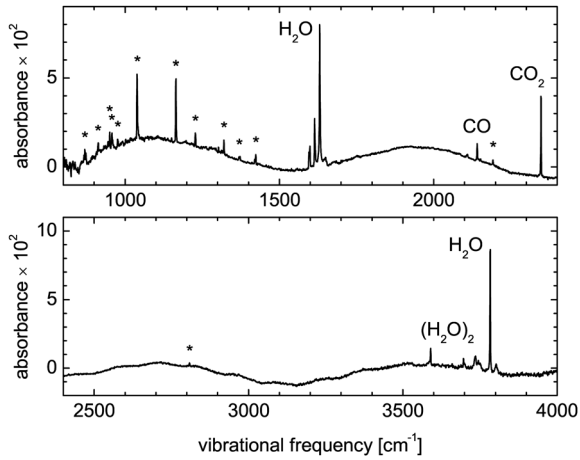

Fig. 4 Infrared absorption features of species isolated in a Ne matrix at 6.3 K following laser vaporization of amorphous $Mg_{0.4}Fe_{0.6}SiO_3$. Asterisks mark the features. The material had been accumulated for 40 min.

On the other hand, there are additional bands at the positions 870, 950, 958, 976, 1369, and 1424 cm^{-1}. After comparison with measurements on species isolated in Ar matrices, we tentatively assign the bands at 1369 and 1424 cm^{-1} to SiO_3 (1363.5 cm^{-1} in Ar matrix) and SiO_2 (1416 cm^{-1} in Ar matrix), respectively.[22] Other tentative assignments would be to FeO (870 cm^{-1} here, 873.08 cm^{-1} in Ar matrix),[23] and OFeO (950 cm^{-1} here, 945.8 cm^{-1} in Ar matrix).[24]

The absorption at 976 cm^{-1} has not been assigned.

3.2 Analysis of the low-temperature condensates

The condensates were studied by IR spectroscopy, high-resolution transmission electron microscopy (HRTEM), and energy dispersive X-ray (EDX) spectroscopy. Generally, IR spectroscopy is the best method to follow up the silicate condensation *in situ* that means independence of the temperature. The formation of the broad silicate bands at about 10 and 20 μm corresponding to the Si–O stretching and bending modes of amorphous silicates is a clear indicator for the first appearance of a solid layer. However, due to the experimental requirements (study of the gaseous precursors and the condensate of one sample *in situ*), the final layer thickness of the condensed silicate was rather small. Therefore, the typical silicate bands were weak and the measurement of the 20 μm band was not possible without having a very low signal to noise ratio.

In each experiment, after annealing and complete evaporation of the Ne atoms, the species constituting the background gas have deposited on the still cold substrate giving various features. Fig. 5 shows spectra obtained with the Mg_2SiO_4 target after evaporation of the Ne atoms and cooling to 6.5 K. Beside the absorption bands due to CO, CO_2, and H_2O, a feature is seen near 1000 cm^{-1}, which we attribute to a solid condensate. The profile of this band is likely affected by the presence of the broad water ice feature that peaks near 780 cm^{-1}.[25] After warming to room temperature, the absorption band attributed to the condensate

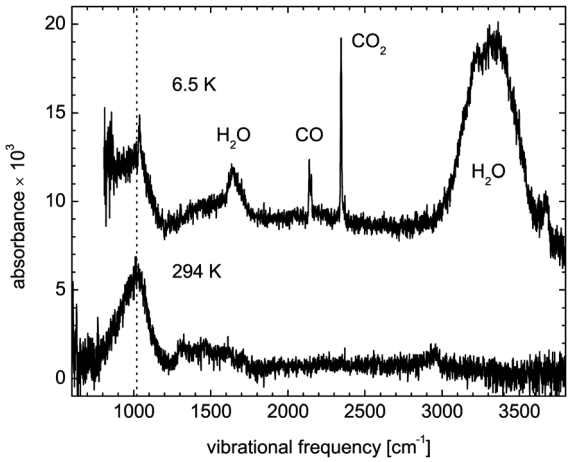

Fig. 5 Infrared spectra of the condensate obtained with the Mg_2SiO_4 target. (Top) Spectrum measured at 6.5 K after warming to 13 K. (Bottom) Spectrum measured at room temperature.

shows an asymmetric profile, which is steeper on the higher frequency side. The maximum of the band is located at ~1020 cm^{-1} (9.8 μm).

Working with the $Mg_{0.4}Fe_{0.6}SiO_3$ target, we did not observe immediately the expected IR absorption near 1000 cm^{-1}, neither at low nor at room temperature. Nonetheless, after the experiment, a solid deposit on the substrate has been detected that has been measured using a clean KBr substrate as reference. A distinct band was observed near 1000 cm^{-1} clearly pointing to the formation of a silicate material. This finding is certainly caused by small problems with the reference measurements of pure KBr during the cooling and warming up phase. Previous temperature-dependent IR measurements of low-temperature SiO_x condensates revealed the formation of the solid phase already at about 10 K.[19] Similarly, the magnesium silicate condensate shown in Fig. 5 has also been formed at low temperature (13 K). Therefore, we act on the assumption that the solid condensate was already formed at low temperature.

Fig. 6 shows IR spectra of final condensates obtained by evaporation of a Mg_2SiO_4 and a $Mg_{0.4}Fe_{0.6}SiO_3$ target, respectively. Both spectra were taken at room temperature. A small shift of the 10 μm band is observed. The bands have their maximum at ~990 cm^{-1} (10.1 μm) and ~1020 cm^{-1} (9.8 μm), respectively. A lower polymerization degree in the condensate produced from a pyroxene-like target ($Mg_{0.4}Fe_{0.6}SiO_3$) should give a band that is shifted to smaller wavelengths compared to those produced from the olivine target (Mg_2SiO_4). The comparison of the bands show that both condensates have to have similar stoichiometry. This has been confirmed by EDX analysis (see Table1).

In addition, the final condensates were studied by high-resolution transmission electron microscopy (HRTEM). HRTEM micrographs of the magnesium iron silicate condensed at low temperatures show fluffy aggregates that are composed of nanometer-sized grains. The sizes of individual primary grains vary between 3 and 15 nm. The internal grain structure is found to be completely amorphous and the final condensate shows a clear homogeneity in structure and

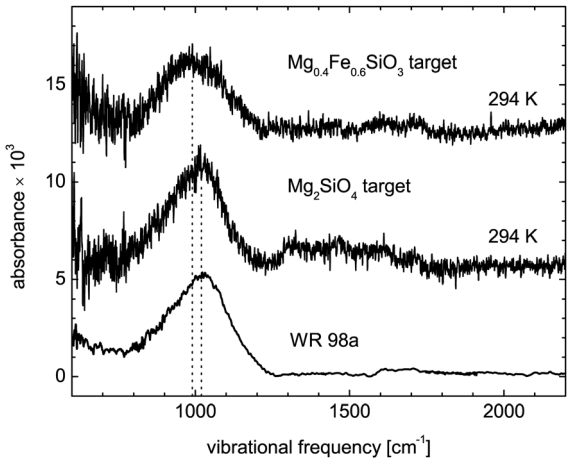

Fig. 6 Infrared spectra of the final condensates obtained by laser-vaporization of amorphous $Mg_{0.4}Fe_{0.6}SiO_3$ and Mg_2SiO_4 targets measured at room temperature. The third spectrum shows the normalized silicate absorption feature toward WR 98a representing the local ISM.[26] The spectra are vertically shifted for clarity.

Table 1 Composition of the condensed silicates by EDX analysis

Condensate	At% Mg	At% Fe	At% Si	At% O
MgFe-silicate	4.9	15.8	17.3	62.0
Mg-silicate	20.8	—	20.9	58.3

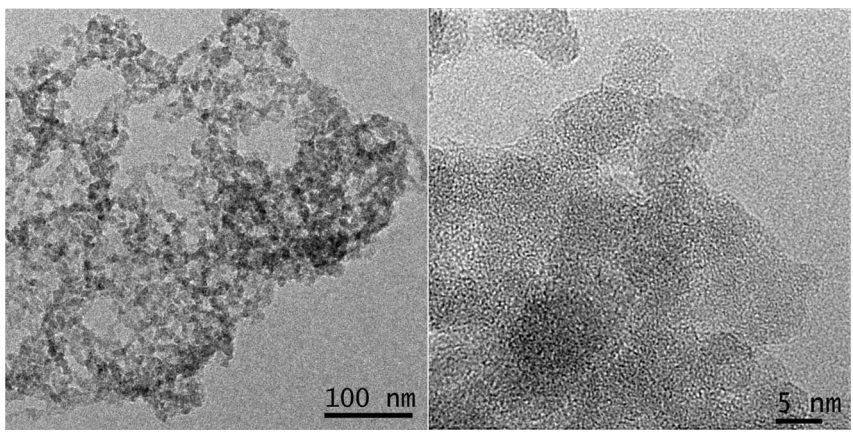

Fig. 7 HRTEM images of the final condensate prepared from the evaporation and recondensation of a magnesium iron silicate at low temperatures. The left image shows an overview of a big cluster. The right image presents a direct view inside the amorphous grains. Please note the irregular structure of the interior of the grains.

composition (see Fig. 7). No hints at phase separations of the MgFe-silicate into individual oxides such as FeO, MgO, and/or SiO_2 can be observed. The morphology and structure of the grains is very similar to the low-temperature

condensate produced from SiO molecules.[4] In addition, very similar results have been obtained for the pure magnesium silicate prepared by laser ablation from a target with the composition Mg_2SiO_4. The formed fluffy aggregates are composed of small primary particles with a completely amorphous structure.

The analytical characterization was complemented by energy-dispersive X-ray spectroscopy (EDX). The method allows the determination of the final composition of the silicate material. The analysis revealed an iron-rich magnesium silicate for the condensate produced from the $Mg_{0.4}Fe_{0.6}SiO_3$ target, the composition of which is given in Table 1. Compared to the composition of the target, the material became poor in magnesium. This is probably due to a selective evaporation process. In an amorphous $Mg_{0.4}Fe_{0.6}SiO_3$ silicate, the MgO represents the most heat-resistant component of the silicate. The composition of the final condensate produced from the Mg_2SiO_4 target is also shown in Table 1. Compared to the target, the condensate is depleted in Mg and shows a pyroxene stoichiometry.

4 Astrophysical discussion

In the ISM, gaseous species may accrete on cold surfaces of pre-existing small particles. The repeated erosion of silicate stardust in SN-induced shock waves is the source of these gaseous species in the ISM. To simulate such processes in the laboratory, we have evaporated silicate dust analogs that have been produced by melting and quenching. These materials have successfully been used to model spectral energy distributions of many astrophysical sources.[27–29] The applied material represents a realistic source for the release of astrophysically relevant gaseous species.

The isolation of the evaporated species in condensed rare gases cools them down before they can interact among each other. This step is necessary as laser-vaporized molecules are hot and their internal energy may affect the chemistry of accretion. The analytical characterization of the species released from silicates and finally embedded in the Ne matrix has shown that beside SiO mainly Mg, Fe, and small molecules such as O_3, O_4^+, SiO_2, SiO_3, FeO, and FeO_2 are precursors of the silicates. It is their accretion that resulted in the formation of silicate grains. While SiO and FeO have been discovered in the ISM,[30–32] the other molecules have not been reported. A model for the chemistry of silicon in dense interstellar clouds includes SiO_2 in its network.[33] The production of SiO by interstellar shocks in molecular outflows predicts the presence of SiO_2.[34]

The condensation of pure silicon monoxide and of more complex silicates with olivine and pyroxene composition by accretion of molecules and atoms on cold surfaces, and subsequent reactions between them at temperatures between 10 and 20 K, has been proven experimentally. The grains were formed by reactions of the embedded molecules during the annealing (10–12 K) and evaporation of the Ne matrix (13 K). The applied conditions are comparable to those prevailing in molecular clouds. The final condensates are fluffy aggregates consisting of small nanometer-sized primary grains. All low-temperature silicates possess amorphous structures and form fluffy aggregates.

The dust condensation at low temperature and low density in the ISM is a process that is discussed to be necessary to keep the balance between dust destruction and formation. So far, there is no exact description of where the cold condensation process may take place. Turbulence in the ISM can quickly

distribute the refractory elements such as Mg, Si, and other species produced in SN shocks into the surrounding medium. In SN ejecta, synthesized materials are mixed by turbulence with the surrounding ISM on a time scale of 100 Myr.[35] One can assume a similar time scale for the mixing of elements liberated from destroyed grains. The process of cold condensation may already be active in diffuse clouds with low temperature and in low-density regions of molecular clouds. In molecular cloud environments with maximum density, where many non-refractory and refractory species and elements may accrete simultaneously on the grains, very complex ices should be formed. There are two competitive processes influencing the growth of the solid layer which are the desorption and the sticking processes. The desorption process is strongly determined by the bonding energy between the species and the surface. According to Draine,[2] for binding energies of 0.1 eV, the lifetime is about 5×10^5 yr. Accreted species that may form strong bonds, which are typical for refractory solids, may grow very fast and remain on the surface for a long time. Diffusion and desorption processes on grain surfaces may finally trigger the formation of more stable siliceous and carbonaceous solids in addition to less stable complex ices. Furthermore, the interstellar UV field and UV photons from young stars inside the clouds, and cosmic rays, can penetrate the interior of such MCs and trigger reactions between accreted molecules and clusters.

Selection processes that may lead to the formation of spatially separated interstellar dust components have to be addressed in upcoming experimental studies.

The condensation of species produced by laser vaporization of silicates has already been studied, albeit under different conditions. The vaporized species were condensed in the gas phase in a quenching gas atmosphere at high temperatures.[36–41] The particles formed in this process were deposited on various substrates before being investigated. The structure and general morphology of the high-temperature and low-temperature siliceous condensates turned out to be remarkably similar. Both are characterized by amorphous structures. In addition, both types of condensates show very similar spectral properties well comparable to the 10 μm profile of the observed interstellar silicates. So far, distinct structural and spectral differences between high- and low-temperature condensates cannot be observed.

5 Conclusions

The condensation of complex silicates with pyroxene composition at temperatures between 10 and 20 K by accretion of molecules and atoms on cold surfaces, and subsequent reactions between them, has been proven experimentally. The experiments clearly demonstrate an efficient silicate formation at low temperatures. The final condensates are fluffy aggregates consisting of small nanometer-sized primary grains. All low-temperature silicates condense in amorphous form and they were found to be homogeneous in structure and composition. To study the gaseous precursors of such condensation processes that can be formed by erosion of dust grains in SN schock waves, we have evaporated glassy silicate materials with a pulsed Nd:YAG laser. The liberated gaseous species were embedded in solid neon matrices that have been studied by spectroscopy in the UV/VIS and IR range. The IR spectral properties of low-temperature siliceous

condensates do not much differ from silicates produced in high-temperature condensation processes. A sound coincidence between the 10 μm band of the interstellar silicates measured by Chiar & Tielens[26] and the 10 μm band of the low-temperature siliceous condensate can be noted.

Acknowledgements

The authors acknowledge the support of the Deutsche Forschungsgemeinschaft through project No. He 1935/26-1 within the framework of the Priority Program 1573 "Physics of the Insterstellar Medium". M. K. is grateful for the award of an Eötvös Scholarship of the Hungarian State.

References

1 S. Zhukovska, H.-P. Gail and M. Trieloff, *Astron. Astrophys.*, 2008, **479**, 453–480.
2 B. T. Draine, *Cosmic Dust - Near and Far*, 2009, p. 453.
3 A. P. Jones and J. A. Nuth, *Astron. Astrophys.*, 2011, **530**, A44.
4 S. A. Krasnokutski, G. Rouillé, C. Jäger, F. Huisken, S. Zhukovska and T. Henning, *Astrophys. J.*, 2014, **782**, 15.
5 J. Dorschner, B. Begemann, T. Henning, C. Jaeger and H. Mutschke, *Astron. Astrophys.*, 1995, **300**, 503.
6 H. Dubost, *Chem. Phys.*, 1976, **12**, 139–151.
7 L. Wan, L. Wu, A.-W. Liu and S.-M. Hu, *J. Mol. Spectrosc.*, 2009, **257**, 217–219.
8 D. Forney, M. E. Jacox and W. E. Thompson, *J. Mol. Spectrosc.*, 1993, **157**, 479–493.
9 A. Kramida, Yu. Ralchenko, J. Reader and NIST ASD Team, *NIST Atomic Spectra Database (ver. 5.1)*, [Online]. Available: http://physics.nist.gov/asd[2014, February 7]. National Institute of Standards and Technology, Gaithersburg, MD., 2013.
10 J. G. McCaffrey and G. A. Ozin, *J. Chem. Phys.*, 1988, **88**, 2962–2971.
11 B. Healy, P. Kerins and J. G. McCaffrey, *Low Temp. Phys.*, 2012, **38**, 679–687.
12 J. Hormes, M. Sauer and R. Scullman, *J. Mol. Spectrosc.*, 1983, **98**, 1–19.
13 P. Brosset, R. Dahoo, B. Gauthier-Roy, L. Abouaf-Marguin and A. Lakhlifi, *Chem. Phys.*, 1993, **172**, 315–324.
14 A. Jaye, W. Laasch and P. Gütler, *Investigations of the Hartley band of ozone isolated in rare gas matrices*, in DESY Photon Science HASYLAB Annual Report, Part 1, Contribution 21-241, 1998.
15 W. E. Thompson and M. E. Jacox, *J. Chem. Phys.*, 1989, **91**, 3826–3837.
16 M. E. Jacox and W. E. Thompson, *J. Chem. Phys.*, 1994, **100**, 750–751.
17 M. E. Jacox and W. E. Thompson, *J. Phys. Chem. A*, 2013, **117**, 9380–9390.
18 R. K. Khanna, D. D. Stranz and B. Donn, *J. Chem. Phys.*, 1981, **74**, 2108–2115.
19 G. Rouillé, S. A. Krasnokutski, M. Krebsz, C. Jäger, F. Huisken and T. Henning, Cosmic dust formation at cryogenic temperatures, in *The Life Cycle of Dust in the Universe: Observations, Theory, and Laboratory Experiments*, ed. A. Andersen, M. Baes, H. Gomez, C. Kemper and D. Watson, PoS(LCDU 2013)047, 2014.
20 J. W. Hastie, R. H. Hauge and J. L. Margrave, *Inorg. Chim. Acta*, 1969, **3**, 601–606.
21 L. Andrews, E. S. Prochaska and B. S. Ault, *J. Chem. Phys.*, 1978, **69**, 556–563.

22 B. Tremblay, P. Roy, L. Manceron, M. E. Alikhani and D. Roy, *J. Chem. Phys.*, 1996, **104**, 2773–2781.
23 D. W. Green, G. T. Reedy and J. G. Kay, *J. Mol. Spectrosc.*, 1979, **78**, 257–266.
24 G. V. Chertihin, W. Saffel, J. T. Yustein, L. Andrews, M. Neurock, A. Ricca and C. W. Bauschlicher, *J. Phys. Chem.*, 1996, **100**, 5261–5273.
25 K. I. Öberg, H. J. Fraser, A. C. A. Boogert, S. E. Bisschop, G. W. Fuchs, E. F. van Dishoeck and H. Linnartz, *Astron. Astrophys.*, 2007, **462**, 1187–1198.
26 J. E. Chiar and A. G. G. M. Tielens, *Astrophys. J.*, 2006, **637**, 774–785.
27 C. Gielen, J. Bouwman, H. van Winckel, T. Lloyd Evans, P. M. Woods, F. Kemper, M. Marengo, M. Meixner, G. C. Sloan and A. G. G. M. Tielens, *Astron. Astrophys.*, 2011, **533**, A99.
28 M. Min, L. B. F. M. Waters, A. de Koter, J. W. Hovenier, L. P. Keller and F. Markwick-Kemper, *Astron. Astrophys.*, 2007, **462**, 667–676.
29 F. J. Molster, L. B. F. M. Waters and A. G. G. M. Tielens, *Astron. Astrophys.*, 2002, **382**, 222–240.
30 R. W. Wilson, A. A. Penzias, K. B. Jefferts, M. Kutner and P. Thaddeus, *Astrophys. J.*, 1971, **167**, L97–L100.
31 C. M. Walmsley, R. Bachiller, G. Pineau des Forêts and P. Schilke, *Astrophys. J.*, 2002, **566**, L109–L112.
32 R. S. Furuya, C. M. Walmsley, K. Nakanishi, P. Schilke and R. Bachiller, *Astron. Astrophys.*, 2003, **409**, L21–L24.
33 E. Herbst, T. J. Millar, S. Wlodek and D. K. Bohme, *Astron. Astrophys.*, 1989, **222**, 205–210.
34 P. Schilke, C. M. Walmsley, G. Pineau des Forêts and D. R. Flower, *Astron. Astrophys.*, 1997, **321**, 293–304.
35 M. S. Oey, *A Massive Star Odyssey: From Main Sequence to Supernova*, 2003, p. 620.
36 J. R. Stephens and R. W. Russell, *Astrophys. J.*, 1979, **228**, 780–786.
37 J. R. Stephens, A. Blanco, E. Bussoletti, L. Colangeli, S. Fonti, V. Mennella and V. Orofino, *Planet. Space Sci.*, 1995, **43**, 1241–1246.
38 J. R. Brucato, L. Colangeli, V. Mennella, P. Palumbo and E. Bussoletti, *Astron. Astrophys.*, 1999, **348**, 1012–1019.
39 J. R. Brucato, V. Mennella, L. Colangeli, A. Rotundi and P. Palumbo, *Planet. Space Sci.*, 2002, **50**, 829–837.
40 C. Jäger, H. Mutschke, T. Henning and F. Huisken, *Cosmic Dust - Near and Far*, 2009, p. 319.
41 T. Sabri, L. Gavilan, C. Jäger, J. L. Lemaire, G. Vidali, H. Mutschke and T. Henning, *Astrophys. J.*, 2014, **780**, 180.

